# The Development of a Finite Volume Method for Modeling Sound in Coastal Ocean Environment

Wen Long, Zhaoqing Yang, Andrea Copping
Pacific Northwest National Laboratory
Marine Sciences Lab
Sequim, WA, USA
Wen.Long@pnnl.gov

Ki Won Jung, Z. Daniel Deng
Pacific Northwest National Laboratory
Energy and Environment Directorate
PO Box 999
Richland, WA, USA, 99352

***Abstract*— *The rapid growth of renewable energy from off-shore sources has raised concerns that underwater noise from construction and operation of offshore devices may interfere with communication of marine animals. An underwater sound model was developed to simulate sound propagation from marine-hydrokinetic energy (MHK) devices or offshore wind (OSW) energy platforms. Finite volume and finite difference methods were developed to solve the 3D Helmholtz equation of sound propagation in the coastal environment. For the finite volume method, the grid system consists of triangular grids in the horizontal plane and sigma-layers in the vertical dimension. A 3D sparse matrix solver with complex coefficients was formed for solving the resulting acoustic pressure field. The Complex Shifted Laplacian Preconditioner (CSLP) method was applied to solve the matrix system iteratively with MPI parallelization using a high performance cluster. The sound model was then coupled with the Finite Volume Community Ocean Model (FVCOM) for simulating sound propagation generated by human activities in a range-dependent setting, such as offshore wind energy platform construction and tidal stream turbine operations. As a proof of concept, initial validation of the finite difference solver is presented for two coastal wedge problems.***

Keywords—***Sound, Coastal Ocean, Finite Volume, Finite Difference, Offshore Wind Energy, Coupling, CSLP, Helmholtz Equation***

## I. INTRODUCTION

Renewable energy generated from offshore resources – by marine energy (waves, tidal streams and ocean currents) and offshore wind energy – has the potential to contribute to the US low carbon "all of the above" portfolio of energy sources. These devices are commonly deployed in estuaries and coastal waters within 20 miles of the coastline. However, stakeholders and regulators have concerns that the extraction of marine renewable energy may pose a risk to the well-being of marine mammals and fish[1][2]. One of the potential risks is from the addition of unnatural sound generated by energy devices that could injure, disorient, or alter the movements of marine animals. The effects of sound from wave and tidal stream devices and sound from pile driving for offshore wind rank as some of the most significant concerns. The effect of sound from marine energy extraction is further exacerbated by a lack of predictive capability to evaluate and understand sound propagation from these sources.

Sound transmission is closely related to ocean water density, which is in turn dependent on water temperature, salinity and pressure (depth) [3]. Typical vertical density stratification due to temperature and salinity in the ocean is described in [4] and simple regression of the data gives sound speed C (m/sec) as

$$C=1507-9.3279(S-35)+2.8941(T-20)+1.7177P/1000000 \tag{1}$$

where S is salinity in practical salinity unit (psu), T is temperature in degrees centigrade, and P is pressure in Pascals. For typical deep ocean areas, the main contribution to variation of sound speed is due to temperature stratification and pressure. This relation sets up a minimum speed at around 700m depth. As an example, sound generated at about 1100m water depth propagates at small angles around the horizontal direction is refracted up and down around the same depth level, resulting in horizontal propagation to very long distances. In coastal zones where salinity could vary from 0 to 35 psu, the variation of C due to salinity could be as much as ±50m/sec. Sound transmission in coastal waters is more temporally and spatially variable than in the open ocean due to seasonal influences of river plumes, effect of meteorological wind stress and heat fluxes, and reflections of sound from complex coastal geometries. An advanced model can be used to account for this variability to accurately predict sound fields. However, coupled hydrodynamic and acoustic modeling has not been developed because the intensive computational resources needed for coupled modeling have not been readily available until the last few years.

We improved the ability to predict sound propagation in coastal regions by providing two major innovations in the field of acoustic modeling: a) formulate the acoustics problem mathematically for meeting the challenges of coupling time domain hydrodynamic model with frequency domain acoustic model and b) coupling of the well-known three dimensional ocean hydrodynamic circulation model FVCOM (Finite Volume Community Ocean Model [5,6,7,16]), which resolves the variations of water density and sea surface elevation, with the acoustic model that solves underwater sound transmission

978-0-933957-43-5 ©2015 MTS

loss, reflection from lateral, bottom and surface boundaries, as well as refraction due to varying density field.

## II. HYDRODYNAMIC MODEL

FVCOM solves the continuity and momentum equations using the finite-volume method and sigma-stretched coordinate transformation in the vertical direction.

### A. *Formulation of Hydrodynamics in FVCOM*

The momentum equations of FVCOM in the horizontal directions have the following general form [5,6,7]:

$$\frac{\partial uD}{\partial t}+\frac{\partial u^2D}{\partial x}+\frac{\partial uvD}{\partial y}+\frac{\partial u\omega}{\partial \sigma}-fvD= -\frac{D}{\rho_o}\frac{\partial p}{\partial x}+\frac{1}{D}\frac{\partial}{\partial \sigma}\left(K_m\frac{\partial u}{\partial \sigma}\right)+DF_x \qquad (2)$$

$$\frac{\partial vD}{\partial t}+\frac{\partial uvD}{\partial x}+\frac{\partial v^2D}{\partial y}+\frac{\partial v\omega}{\partial \sigma}+fuD= -\frac{D}{\rho_o}\frac{\partial p}{\partial y}+\frac{1}{D}\frac{\partial}{\partial \sigma}\left(K_m\frac{\partial v}{\partial \sigma}\right)+DF_y \qquad (3)$$

where ($x$, $y$, $\sigma$) are the east, north, and vertical axes in the Cartesian coordinates; ($u$, $v$, $\omega$) are the three velocity components in the $x$, $y$, and $\sigma$ directions; $D$ is total water depth; ($F_x$, $F_y$) are the horizontal momentum diffusivity terms in the $x$ and $y$ directions; $K_m$ is the vertical eddy viscosity coefficient; $\rho$ is water density; $p$ is pressure; and $f$ is the Coriolis parameter. $\sigma$ is stretched vertical coordinate system based on an algebraic transformation from vertical Cartesian coordinate $z$:

$$\sigma=\frac{z-\xi}{D}, \qquad (4)$$

with $\xi(t,x,y)$ being the surface elevation and $D=h+\xi$, where $h(x,y)$ is still water depth. The surface and bottom boundaries are corresponding to $\sigma=0$ and $\sigma=-1$ respectively. Similarly the temperature $T(x,y,z,t)$ and salinity $S(x,y,z,t)$ are solved in 3D using the following transport equations:

$$\frac{\partial TD}{\partial t}+\frac{\partial uTD}{\partial x}+\frac{\partial vTD}{\partial y}+\frac{\partial \omega T}{\partial \sigma}= \frac{1}{D}\frac{\partial}{\partial \sigma}\left(K_T\frac{\partial T}{\partial \sigma}\right)+D\widehat{\mathrm{H}}+DF_T \qquad (5)$$

$$\frac{\partial SD}{\partial t}+\frac{\partial uSD}{\partial x}+\frac{\partial vSD}{\partial y}+\frac{\partial \omega S}{\partial \sigma} =\frac{1}{D}\frac{\partial}{\partial \sigma}\left(K_S\frac{\partial S}{\partial \sigma}\right)+DF_S \qquad (6)$$

where $\widehat{\mathrm{H}}(x,y)$ is heating source/sink for a given vertical location; $F_T$ and $F_S$ are the horizontal eddy diffusion terms for temperature and salinity respectively; $K_T$ and $K_S$ are for vertical eddy diffusivity of temperature and salinity. The above equations are solved using finite volume integration based on spatial discretization with triangular meshes in horizontal plane $(x,y)$ and fixed $\sigma$ layers in vertical direction. For derivations of the discretized system, readers are referred to [5,6,7] for details.

### B. *Application of FVCOM for a Coastal Wedge Case with a River Plume*

A typical coastal wedge application is depicted in Fig. 1. The water depth at the shoreline (right hand side) is 2 meters, and the shoreline is about 2km long. The cross shore bathymetry is described as a piece-wise linear slopping bottom with maximum depth at the open boundary being 44m. A river discharge of $150\ m^3/sec$ is placed at the center of the coastal line and brings a freshwater plume to the coastal zone. For such a relatively simple geometry, a grid mesh is chosen such that all the triangular nodes are collapsing with a structured mesh. The FVCOM model is run for 39 days with time step $\Delta t=1sec$ from initially evenly distributed salinity of 30 $psu$ and quiescent flow field ($(u,v,\omega)=0$). Salinity distribution at the last hour of the 39-day simulation is plotted using colored contours (Fig.1). For simplicity, Coriolis forcing is set to zero and temperature simulation is disabled.

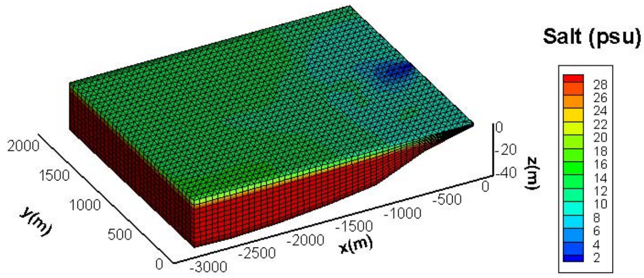


Figure 1. Coastal wedge simulation of river plume

## III. COASTAL ACOUSTIC MODEL

### A. *Mathematical Description of Sound in Coastal Oceans*

In Cartesian coordinates $(x,y,z)$, the pressure disturbance caused by sound in ocean $p(x,y,z,t)$ is governed by the following 3D wave equation

$$\frac{\partial^2 p}{\partial t^2}-C^2\nabla^2 p=F(x,y,z,t) \qquad (7)$$

where $C(x,y,z)$ is sound speed ($unit{:}\, m/s$) and $F$ is the sound source strength. For a given frequency $f$, the pressure $p$ can be written in harmonic form (using complex numbers, and the physical pressure will always be the real part of the complex number)

$$p(x,y,z,t) = \hat{p}(x,y,z)e^{i\varpi t} \qquad (8)$$

Substituting this harmonic equation into (7), the Helmholtz equation is obtained

$$\nabla^2\hat{p} + k^2\hat{p} = -\frac{1}{C^2}\hat{F} \qquad (9)$$

where $F = \hat{F}e^{i\varpi t}$ and $\varpi = 2\pi f$ is the angular frequency, and $k(x,y,z) = \frac{\varpi}{C}$ is the angular wave number. In coastal oceans, $C$ and $k$ are spatially variable due to the variation of temperature and salinity. For applications with attenuation, $k^2$ is replaced by $(1-\alpha i)k^2$, where $\alpha$ is attenuation coefficient and $i$ is the notation for the imaginary part of a complex number.

Similar to derivation of momentum equations as well as non-hydrostatic pressure Poisson equation [9] in Sigma coordinates $(x,y,\sigma)$, by using the coordinate transform $(x,y,z,t) \to (x',y',\sigma,t')$, where $x' = x$, $y' = y$, $\sigma = \sigma(x,y,t) \equiv (z-\xi)/D$, equation (9) can be re-written in as

$$\nabla_{h\sigma}{}^2\hat{p} + \left({A_1}^2 + {A_2}^2 + \frac{1}{D^2}\right)\frac{\partial^2\hat{p}}{\partial\sigma^2} + \left(\frac{\partial A_1}{\partial x'} + \frac{\partial A_2}{\partial y'}\right)\frac{\partial\hat{p}}{\partial\sigma} + 2A_1\frac{\partial^2\hat{p}}{\partial x'\partial\sigma} + 2A_2\frac{\partial^2\hat{p}}{\partial y'\partial\sigma} + k^2\hat{p} = -\frac{1}{C^2}\hat{F} \qquad (10)$$

where $\nabla_{h\sigma}{}^2$ is the horizontal (2D) Laplacian operator in $(x',y',\sigma,t')$ coordinates:

$$\nabla_{h\sigma}{}^2 = \left(\frac{\partial^2}{\partial x'^2} + \frac{\partial^2}{\partial y'^2}\right)|_{\sigma=const} \qquad (11)$$

and

$$A_1 = -\frac{1}{D}\left(\frac{\partial\xi}{\partial x'} + \sigma\frac{\partial D}{\partial x'}\right) \qquad (12)$$

$$A_2 = -\frac{1}{D}\left(\frac{\partial\xi}{\partial y'} + \sigma\frac{\partial D}{\partial y'}\right) \qquad (13)$$

For convenience, we will use $x$ for $x'$, $y$ for $y'$ and $t$ for $t'$.

### B. Finite Volume Formulation

Equation (10) can be integrated in 3D over the volume $\mathbb{V}_{jr}$ confined by $r'th$ sigma layer with surface domain size $\Omega_j$ for the area formed by nodes surrounding node $j$, where $r = 1$ for the top layer and $r = L-1$ for the bottom layer (Fig. 2). The vertical extent is split into totally $L$ levels indexed by $l$, with $l = 1$ for the top level (surface elevation) and $l = L$ for the bottom level ($z = -h$, i.e. $\sigma = -1$) .

The integration over $\mathbb{V}_{jr}$ is written as

$$\iiint_{\mathbb{V}_{jr}}\left[\nabla_{h\sigma}{}^2\hat{p} + \left({A_1}^2 + {A_2}^2 + \frac{1}{D^2}\right)\frac{\partial^2\hat{p}}{\partial\sigma^2} + \left(\frac{\partial A_1}{\partial x'} + \frac{\partial A_2}{\partial y'}\right)\frac{\partial\hat{p}}{\partial\sigma} + 2A_1\frac{\partial^2\hat{p}}{\partial x'\partial\sigma} + 2A_2\frac{\partial^2\hat{p}}{\partial y'\partial\sigma} + k^2\hat{p}\right]dxdyd\sigma = -\iiint_{\mathbb{V}_{jr}}\frac{1}{C^2}\hat{F}\ dxdyd\sigma \qquad (14)$$

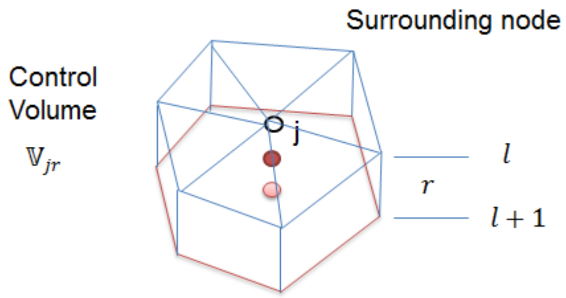


Figure 2. Control volume of a layer $r$ confined by two vertical levels $l$ and $l+1$, with the circle indicating node $j$

Carrying out the integration term by term, similar to the derivations in [9], using Stokes theorem and assuming surface boundary condition as $\hat{p}|_{\sigma=0} = 0$, the discretized system can be arranged to arrive a matrix equation for all $\hat{p}$ values on all nodes $j = 1,\dots,N$, and all levels $l = 1,\dots,L$

$$A\hat{p} = b \qquad (15)$$

where $A$ is an NL by NL sparse matrix.

### C. Finite Difference Formulation

For implementation with structured grid system of constant grid spacing $\Delta x$, $\Delta y$, $\Delta z$ in a 3D regular box-shaped domain with discretized $\hat{p}$ values indexed by $(i,j,l)$ in $x,y,z$ directions . Equation (9) can be discretized using the finite difference method as

$$\frac{(\hat{p}_{\,i-1,j,l} - 2\hat{p}_{\,i,j,l} + \hat{p}_{\,i+1,j,l})}{\Delta x^2} + \frac{(\hat{p}_{\,i,j-1,l} - 2\hat{p}_{\,i,j,l} + \hat{p}_{\,i,j+1,l})}{\Delta y^2} + \frac{(\hat{p}_{\,i,j,l-1} - 2\hat{p}_{\,i,j,l} + \hat{p}_{\,i,j,l+1})}{\Delta z^2} + k^2\hat{p}_{\,i,j,l} = -\frac{1}{C^2}\hat{F}_{i,j,l} \qquad (16)$$

where $i = 2\dots,M-1$, $j = 2\dots,N-1$, $l = 2\dots,L-1$ and $M,N,L$ are the number of grid points in $x,y,z$ directions respectively. Also, the surface boundary condition is $\hat{p}_{\,i,j,l=1} = 0$. Equation (16) can also be arranged in the form of (15) for all $\hat{p}$ values.

### D. Iterative Helmholtz Solver Based on Complex Shifted Laplacian Preconditioning (CSLP) method

The matrix $A$ is typically a very large sparse matrix of complex numbers. For high frequency sound and large domain, the matrix equation (15) becomes difficult to solve directly. The Complex Shifted Laplacian Preconditioning (CSLP) method by [8] applied along with Bi-CGSTAB[10] or GMRES[15] is used for this research. The method is based on construction of a preconditioning matrix $M_P$

$$M_P = B + (\beta_1 + i\beta_2)k^2I \qquad (17)$$

where $I$ is unit matrix, and $B = A - k^2I$. Instead of solving (15), the following left-preconditioned equation is solved.

$$M_P{}^{-1}A\hat{p} = M_P{}^{-1}b \qquad (18)$$

$\beta_1$ and $\beta_2$ have been optimized for best convergence rate. In our simulations we used $\beta_1 = 0$ and $\beta_2 = 0.5$ . $M_P{}^{-1}$ is simply calculated using an SOR [13] iteration method. To solve for $\hat{p}$ from (18), the Krylov subspace methods called Bi-CGSTAB [10] or GMRES [15] is applied, which are implemented in the PETSc parallel computation library (version 3.6.0)[11].

*E. Radiation Boundary Treatment*

The radiation boundary is needed for open domain simulations. However, because an imperfect radiation condition can reflection in the simulation domain of interest, a treatment that makes the sound wave not return should be applied. This is implemented using the Perfectly-Matching-Layer (PML) method [14]. One typically places 50 grids at the open boundary to absorb outgoing sound waves with a large damping term. Within the PML zone, $k^2$ in (9) is replaced by $(1 - i\alpha)k^2$ , where $\alpha$ is the attenuation factor in the PML zone, which was ramped up from zero at the physical domain boundary to 0.475 at the end of the PML layer. The external boundaries of the PML layers were terminated by the first order Sommerfeld radiation boundary condition, defined as $\frac{d\hat{p}}{dn} = ik\hat{p}$, where $n$ is the normal direction to the boundary.

Fig.3 depicts the $\hat{p}$ solution of a 2D simulation using the PML layer in a homogeneous (uniform sound speed) domain with open boundaries. It demonstrated that our implementation of the PML layers have effectively removed artificial reflections from boundaries.

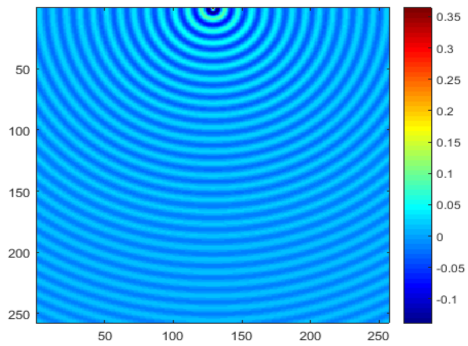


Figure 3. 2D benchmark testing of PML for absorbing sound waves at the boundary. The real part of the pressure is shown in a 2D homogeneous medium with the wavenumber of 0.4189 with PML (not shown). The number of grid points per wavelength is set at 10. The point source is placed on the top line of the figure.

## IV. Application in Idealized Coastal Wedge Examples

The application of finite difference scheme (16) along with CSLP method (18) is presented for two idealized coastal wedge examples. The validation and application of finite volume scheme (14) will be published separately.

*A. 3D ASA Wedge*

Lin et al 2012 [12] discussed simulation of sound in a coastal wedge (called ASA wedge here) using several Parabolic Equation based methods. Here, the same wedge is constructed and simulated. Fig. 4 shows the straight wedge shape coastal zone with shoreline depth of zero and an offshore depth of $200m$, a cross shore distance of $4km$ and an along shore distance of $20km$. A unit sound source of frequency $f = 25Hz$ is placed at $x = -2000m, y = 0m, z = -50m$ (shown as the red sphere in fig. 4). The water is assumed to be uniform in density and with sound speed $C = 1500m/sec$, the seabed is also included and extends to $z = -200m$ with sound speed being $C = 1700m/sec$. PML zones are added for all lateral sides and bottom (not shown) for the simulation.

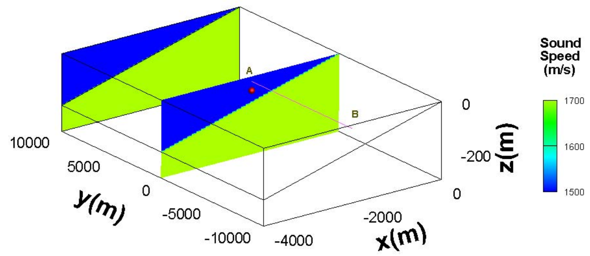


Figure 4. Geometry and sound speed profile of ASA wedge, sound source location is indicated by a sphere below point 'A'.

Fig. 5 shows the computed transmission loss (TL), which is defined as

$$TL = -20log_{10}|\hat{p}| \qquad (19)$$

at $= -15m$ , i.e. $15m$ below surface. In order to obtain the TL value directly, $\hat{p}$ is scaled by pressure at the distance of 1 m from the acoustic source. We see that there is a significant reflection from shoreline. Fig. 6 shows the vertical transect view of XZ plane at $y = 0$. We see that the sound penetrates into the seabed below the sound source. There is also considerable penetration on the shoreline, whereas the area below the seabed off-shore is sheltered.

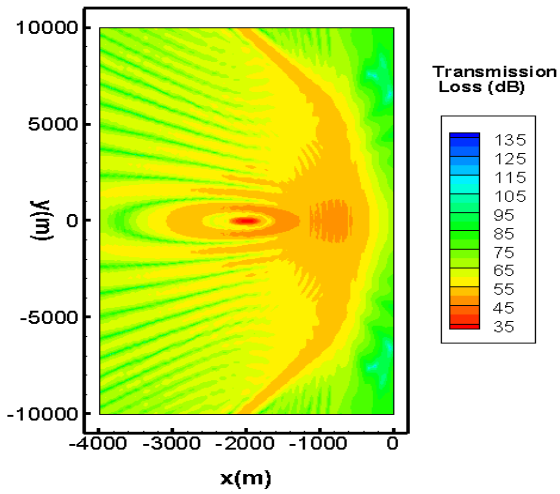


Figure.5. Transmission Loss of XY Plane at z = -15m

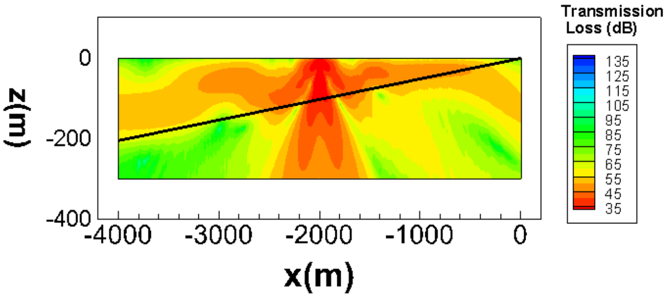


Figure 6. Transmission Loss of XZ Plane Results at y=0m; the dark line indicates the seabed

Fig. 7 shows the transmission loss along line AB of Fig. 4, which is located $15m$ below the surface.

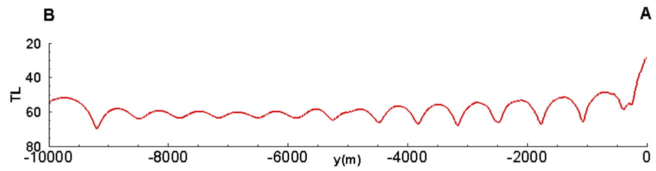


Figure 7. Transmission Loss along line AB at z=-15m (35m above source)

## B. *Coastal Wedge with a River Plume*

The model simulation of the coastal wedge (Fig.1) provided the salinity field with a constant temperature of $20\ ^{o}C$. These results are then used in (1) to calculate the sound speed profile. A unit sound source of frequency $f = 100Hz$ is placed $22.5m$ below the surface. The finite difference scheme formulation (16) is applied with uniform grid size $\Delta x = \Delta y = \Delta z = 1.5m$ for the domain with seabed extended below the maximum water depth ($44m$ deep at the open boundary) to $z = -164m$ with sound speed $C = 2500m/sec$ below seabed. There are also 50 PML grids added in all lateral boundaries and below the extended seabed for this test case. The simulation is carried out using 15 parallel computer nodes of 16 cores each. The model run-time is about 2 hours for a 39-day simulation. Fig. 8 shows the plane (XY) view of transmission loss at $z = -30m$,i.e. $7.5m$ below the source for the sound speed field corresponding to the last hour of hydrodynamic simulation in day 39 (Fig.1). Fig.9 shows the XZ plane view at $y = 1000m$, at the middle of the shoreline. Similar to the wedge of Fig. 6, the sound penetrates into the seabed. There are multiple reflections by the shore line, ocean surface and seabed which formed standing wave patterns. Fig. 10 shows the difference of transmission loss between a fully developed river plume condition and the initial uniform condition ($T = 20\ ^{o}C$ and $S = 30psu$) at $z = -30m$. The presence of river plume changes the sound field significantly.

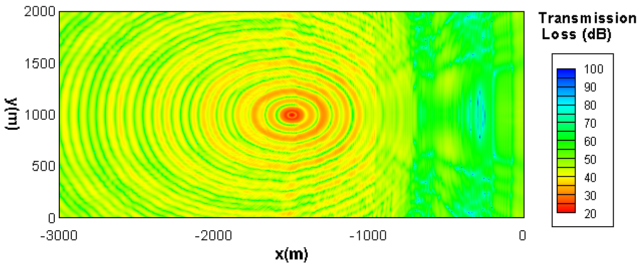


Figure 8. Transmission loss (TL) at z=-30m based on hydrodynamic prediction of sound speed field at end of 39-day simulation (Fig.1)

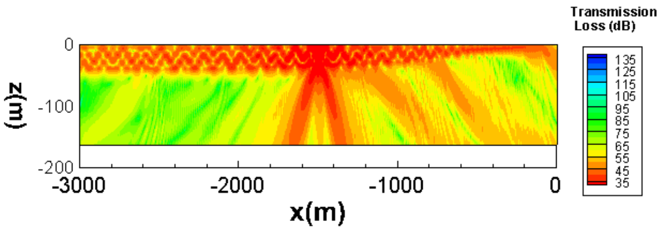


Figure 9. Transmission loss (TL) for the XZ plane at y=1000m based on hydrodynamic prediction of sound speed field at end of 39-day simulation.

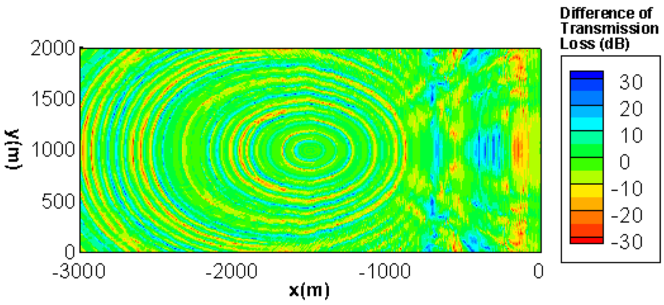


Figure 10. Difference of transmission loss between using hydrodynamic predictions of sound field at end of 39-day (with river plume) and initial state (T=20 and S=30psu) when there is no river plume.

## V. CONCLUSION AND FUTURE WORK

An underwater sound model with finite volume and finite difference methods was developed to simulate sound transmission in the coastal ocean. The hydrodynamic model FVCOM was used to simulate the varying coastal water density distribution and provide the sound speed in the coastal environment. The CSLP solver is used for fast iteration to solve the resulting large and sparse matrix system on a parallel cluster. The validation of finite difference is presented using two wedge cases. This underwater sound model will be useful for evaluating impacts on marine mammals due to construction of OSW energy platforms and deployment of MHK energy devices in coastal regions. Our future work includes validation of the finite volume solver using idealized cases, further validation using field observations in Puget Sound and coupling of the sound model with a marine mammal tracking model.

## ACKNOWLEDGMENT

This study was funded by the Pacific Northwest National Laboratory's Laboratory Directed Research and Development program under project number #66978.

## REFERENCES


[1] Bailey, H., Impacts of wind turbine construction on marine mammals: what can be done? Wind Farm Construction, Ref. No. [UMCES]CBL 12-017, Volume 6, Issue 1, 2012

[2] National Research Council, Marine Mammal Populations and Ocean Noise: Determining When Noise Causes Biologically Significant Effects, Committee on Characterizing Biologically Significant ,Marine Mammal Behavior, http://www.nap.edu/catalog/11147.html, 2005

[3] Lurton, X., An introduction to underwater acoustics, Springer, 2002

[4] Talley LD., Pickard GL, Emery WJ. Swift JH., Descriptive Physical Oceanography, sixth edition, Elsevier, 2011

[5] Chen C, Liu H, Beardsley RC (2003) An unstructured, finite-volume, three-dimensional, primitive equation ocean model: application to coastal ocean and estuaries. J Atmos. Ocean Tech. 20:159–186

[6] Chen, C.; Huang, H.; Beardsley, R.; Liu, H.; Xu, Q.; Cowles, G. A finite volume numerical approach for coastal ocean circulation studies: Comparisons with finite difference models. *Journal of Geophysical Research* 2007, 112, C03018. doi:10.0129/2006JC003485.

[7] Chen, C.; Beardsley, R.C., Cowles, G. An unstructured grid, finite-volume coastal ocean model: FVCOM user manual, School for Marine Science and Technology, University of Massachusetts Dartmouth, 2006, 315pp.

[8] Vuik C,, Erlangga Y.A., Oosterlee C. W., Shifted Laplace preconditioners for the Helmholtz equations, Report# 03-18, ISSN 1389-6520, Delft University of Technology, 2003.

[9] Lai Z., Chen C., Colwes G. W., Beardsley R. C., A nonhydrostatic version of FVCOM, 1. Validation experiments, Journal of Geophysical Research, V15, C11010, doi:10.1029/2009JC005525, 2010

[10] Van de Vorst H.A., Bi-CGSTAB: a fast and smoothly converging variant of Bi-CG for solution of non-symmetric linear systems. SIAM J. Sci. Stat. Comp., 13:631-644, 1992

[11] Balay, S. et al., PETSc Users Manual, Report# ANL-95/11 Rev 3.6, Argonne National Laboratory, June 2015

[12] Lin Y., Colis J. M., Duda T. F., A three-dimensional parabolic equation model of sound propagation using higher-order operator splitting and Pade approximants, JASA Express Letters, October 2012 http://dx.doi.org/10.1121/1.4754421,

[13] Yong D. M., Iterative Solution of Large Linear Systems, Academic Press, 1971

[14] Chew W.C., and W. H. Weedon (1994). "A 3d perfectly matched medium from modified Maxwell's equations with stretched coordinates". *Microwave Optical Tech. Letters* **7** (13): 599–604. doi:10.1002/mop.4650071304

[15] Sadd Y. and M. H. Schultz, GMRES: A generalized minimal residual algorithm for solving nonsymmetric linear systems. SIAM J. Sci. Stat. Comput., 7:856-869, 1986

[16] Yang, Z., T. Wang, N. Voisin and A. Copping, 2015. Estuarine Response to River Flow and Sea-Level Rise under Future Climate Change and Human Development, Estuarine, Coastal and Shelf Sciences. 156, 19-30. DOI: 10.1016/j.ecss.2014.08.015